# Dynamics of distorted cholesterics in a mesogenic versus isotropic polymer network

Kyongok Kang* and Samuel Sprunt†
*Department of Physics, Kent State University, Kent, Ohio 44242, U.S.A.*
(Received 18 April 2005; published 9 September 2005)

The dynamics of the distorted cholesteric director is studied in a complex matrix, such as mesogenic and istotropic polymer networks, by means of dynamic light scattering. We employ polymer-stabilized cholesteric diffraction gratings as our system to measure thermal flutuations of the cholesteric director in photostabilized low-molecular-weight polymer networks. The relaxation rates of fast and slow dynamical modes of the distorted cholesteric directors are measured in two scattering geometries, where the scattering vector is either parallel or perpendicular to the helical axis. The dispersion relations for fluctuation wave vectors along the helical axis are found to be fundamentally different for the two types of polymer networks. Experimental dispersion curves are in agreement with the theoretical predictions developed in the present paper. A possible understanding of dispersion in distorted cholesterics is developed and the experimental results for polymer stabilized cholesteric diffraction gratings are presented in this report. We also discuss the coupling of a slow relaxation mode of distorted cholesterics in a mesogenic versus isotropic polymer network.

DOI: 10.1103/PhysRevE.72.031702 PACS number(s): 83.80.Xz, 42.70.Df, 82.35.−x

## I. INTRODUCTION

There is an increasing interest in cholesteric liquid crystals due to their helicoidal periodic structures in materials science involving photonic band-gap materials [1–3] and in the structure and dynamics of biological membranes [4] and biofunctional surfactants in complex media [5]. Furthermore, polymer-stabilized cholesteric diffraction gratings are electro-optical switching devices that incorporate highly diffractive optical elements. The dynamical mode of the cholesteric director has been described by de Gennes and Prost for an ideal helix [6] and developed by Meyer for distorted cholesteric structures by an external field [7]. Director structures of cholesteric diffraction gratings are simulated by Shiyanovskii *et al.* [8]. The details of the preparation and morphology of polymer-stabilized cholesteric diffraction gratings are discussed in Refs. [9,10], and the difference of optical morphologies of cholesterics in mesogenic versus isotropic polymer networks is also shown in Ref. [11]. In this report, we discuss the relaxation behavior of the distorted cholesteric director in polymer-stabilized networks with dynamic light scattering. Two scattering geometries are used for probing the thermal fluctuations of the cholesteric director. We also use mesogenic versus isotropic type of monomers to investigate their polymer-wall anchoring effect on the cholesteric liquid-crystal host. Therefore, we address the dispersion of the director modes of distorted cholesteric in complex polymer networks and possible confinement effects of polymer walls.

*Corresponding author: Current address: Forschungszentrum Juelich, IFF-Weiche Materie, D-52425, Juelich, Germany. Electronic address: k.kang@fz-juelich.de
†Electronic address: sprunt@physics.kent.edu

## II. EXPERIMENTS

### A. Samples

Cholesteric liquid crystals are prepared by adding the chiral dopant Merck R-1011 to the commercial nematic liquid crystal Merck BL006 (nematic-isotropic transition range ~113 °C). We used two different types of diacrylate monomers in low concentration (~3 wt %): the reactive mesogenic monomer Merck RM257 and the isotropic monomer HDDA. A small amount of photoinitator Irgacure 651 (Ciba Additives) was mixed in at 5 wt % of the monomer concentration (or 0.15–0.25 wt % of the mixture) in order to facilitate the polymerization reaction. HDDA is isotropic at room temperature, and RM257 has the phase sequence crystal-(70 °C)-nematic-(120 °C)-isotropic. All compounds are mixed until each component dissolves uniformly and thoroughly by either a mechanical rotation with a "thermister" (type 16700 mixer) or solvent method. The photostabilization is done by a UV lamp at 365 nm wavelength and 0.04 $mW/cm^2$ for 30 min. The mixture of planar polymer-stabilized gratings is BL006, 7.5 wt % of chiral dopant and 3 wt % reactive monomer (RM257 and HDDA). For a homeotropic boundary condition of the cholesteric sample, the mixture is BL006, 11 wt % of chiral dopant. In order to be able to perform dynamic light scattering, it is important to achieve a pitch that is comparable to the wavelength of the incident beam. Both the mesogenic and isotropic polymer-stabilized cholesteric diffraction gratings have a $2\pi$ pitch of approximately 2.4 $\mu$m. Homemade cells with ~3-$\mu$m spacers were used in place of commercial electro-optic cells. An applied electric ac field of 3–4 V, and frequency ~1 kHz was used to form the initial polymer-stabilized cholesteric diffraction grating texture in the narrower cells. The texture was stabilized over the full $25\times25$ $mm^2$ area of the cell using a UV lamp, collimating lens, and a bandpass filter [365 nm center, 10 nm full width at half maximum (FWHM)]. The optical texture of the homeotropic cholesteric has a $2\pi$ pitch of approximately 3.3 $\mu$m, and the substrate separation is ~5 $\mu$m.

 

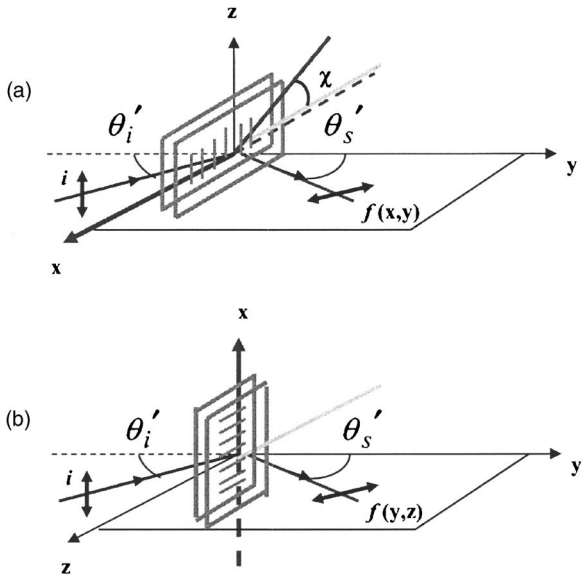


FIG. 1. The schematic drawings of the two scattering geometries: (a) scattering vector $k=k_x$, along the helical axis in the scattering plane for scattering geometry 1, and (b) scattering vector $k=k_z$, perpendicular to both the helical axis and the scattering plane for scattering geometry 2. The $y$ direction is along the substrate normal and the $x$ direction along the helical axis. The arrows $i$ and $f$ represent the initial and final polarizations, respectively. The primed angles ($\theta''$) refer to the laboratory frame with the subscript $i$ and $s$ referring to "incident" and "scattered" light, respectively. To avoid strongly scattered diffraction peaks, we kept the $\chi$ angle at approximately 10° in scattering geometry 1 in (a).

### B. Scattering geometries

For an optically isotropic sample, the incident and scattered vectors have the same length, but differ in a birefringent sample. However, as long as the optic axis is uniform in the birefringent case, but the fluctuations are not confined. The connection between the spectrometer parameters $k_i$ and $k_f$ and the sample fluctuation wave vecotor $q$ can be given by $q=k_f-k_i$. Thus, by controlling the scattering geometry, one normally selects scattering from a specific fluctuation wave vector. Varying this and recording the time correlation function of the scattered intensity then allows to measure the $q$ dependence or dispersion of the relaxation rates (damping constants) of the overdamped fluctuations. Two scattering geometries are used for probing the wave vector dependence of distorted cholesterics, shown in Fig. 1. We will take $y$ as the substrate normal and $x$ as the grating axis. Furthermore, the primed angles $\theta''$ refer to the laboratory frame while the unprimed $\theta$ refers to inside the sample. In scattering geometry 1, where the grating axis is in the scattering plane, the components of the scattering vector can be expressed as

$$k_x^2 = \left(\frac{2\pi}{\lambda_0}\right)^2 (n_s \sin\theta_s + n_i \sin\theta_i)^2 = \left(\frac{2\pi}{\lambda_0}\right)^2 (\sin\theta_s' + \sin\theta_i')^2,$$

$$k_y^2 = \left(\frac{2\pi}{\lambda_0}\right)^2 (n_s \cos\theta_s - n_i \cos\theta_i)^2 = \left(\frac{2\pi}{\lambda_0}\right)^2 (\sqrt{n_s^2 - \sin^2\theta_s'} - \sqrt{n_i^2 - \sin^2\theta_i'})^2,$$

$$k_z^2 = 0. \quad (1)$$

On the other hand, the grating axis is perpendicular to the scattering plane for scattering geometry 2, where $k_x^2=0$, and the other scattering vector components are given by

$$k_y^2 = \left(\frac{2\pi}{\lambda_0}\right)^2 (\sqrt{n_s^2 - \sin^2\theta_s'} - \sqrt{n_i^2 - \sin^2\theta_i'})^2,$$

$$k_z^2 = \left(\frac{2\pi}{\lambda_0}\right)^2 (\sin\theta_s' + \sin\theta_i')^2,$$

where $n_i$ and $n_s$ are indices of refraction for the polarization of the incident light and of the scattered light, respectively. Then we chose depolarized orthogonal orientations of director scattering as the incident polarization $\hat{i}$ perpendicular to the scattering plane and the polarization of the detected light $\hat{f}$ in the scattering plane.

### C. Dynamic light scattering setup

The light source is a symmetric $TEM_{00}$-mode He—Ne laser (a Spectra-Physics model 127 rated at 35 mW), and the laser power at the sample was approximately 5 mW. The laser power was continuously monitored by a photodiode, and all measurements were normalized to eliminate effects due to power drift. The incident and scattering angles were varied by placing the sample on a two-stage, manually adjusted goniometer. Various translation stages allowed us to center the illuminated volume on the rotation axis and to vary the position of the illuminated spot on the sample. We choose the focal length of the entrance lens and the design of the collection apertures as much as possible into a single (or a few) coherence areas. For a given scattering geometry, we may think of the scattering process as diffraction from a transient grating with wave vector $q$ and size comparable to the illuminated sample size $d$ (controlled by the entrance lens). The angular width of the central peak in the diffraction pattern in this case is $\sin\theta \approx \lambda/d$, which defines a coherence angle $\theta$. In our scattering experiment, the incident beam was focused to roughly 150 $\mu$m at the sample, and several coherence areas were collected. The pulse width out of the PAD is typically 5–10 nsec, but in the autocorrelation experiment, the measuring time correlation between pulses generated is the limiting to the photomultiplier tube (PMT) dead time (~100–200 nsec). We used a PMT module (Electron Tubes model P30CWAD5F), designed for single-photon counting and low dark count (<25 cps), and the tube had internal circuits built in the PAD for generating a 1.6-kV operating voltage. For our studies, autocorrelation is adequate for the fluctuations of interest in cholesteric director fluctuations, which are on the msec time scale. Three different correlators were used: The first was an instrument designed and constructed by Dr. A. Baldwin at Kent State. This instrument computes $\langle I(0)I(t)\rangle$ according to the following set of delay time $t-10$ consecutive channels at 50 nsec, 100 $\mu$sec spacing in fast and slow channels. The other two correlators are commercial instruments: The BI9000 from Brookhaven Instruments has a flexible delay time layout, and we used the

following set: over 10 decades, dynamic range 25 nsec/1310 sec. The Flex 2K-12Dx2 from Flexible Instruments has a fixed layout: 36 groups of 8 bins (288 bins total, dynamic range from 12 nsec to 3200 sec). We also used a temperature-controlled stage with a homemade oven with optical access of 0–70° for the scattering angle and 0–45° for the incident angle. The oven was heated by passing a current through a resistive foil heater, which was regulated by a standard bridge circuit with closed loop feedback designed by Professor J. D. Litster of MIT. A thermistor (100 kΩ at 25 °C) was used as the control element in the bridge circuit, and the temperature could be set either by a precision resistor decade box or by an external sweep voltage. A calibrated ultrastable thermistor (125 kΩ at 25 °C, Thermometrics) was used to measure temperature. The measurement thermistor was placed just under the outer glass surface of the sample cell. The short-term stability of our oven was ~10 mK over ~5 min; ~50 mK stability was obtained over ~5 h. The operating range was 25–125 °C. For each scattering geometry, correlation functions have been collected as a function of temperature using the LABVIEW software (National Instruments) to control the correlator, set the temperature through a 16-bit digital-to-analog converter (DAC) used to sweep the temperature controller output and to monitor the temperature through a $5-\frac{1}{2}$-digit multimeter (Keithley model 197A), which measured the voltage drop associated with a constant current of 1 $\mu$A passing through the measurement thermistor.

## III. DIRECTOR FLUCTUATIONS IN CHOLESTERICS

The dynamical properties of cholesteric director fluctuations are described for the fluctuation wave vector $q$ by de Gennes and Prost [6], depending on the director mode that is "umbrella" like or "twisting" around the helical axis. The cholesteric director vector field is defined as each angular rotation $v$ and $u$, for "umbrella" like or "twisting," respectively. When the helical axis is assumed along the $x$ direction, one can express the cholesteric director vector field as

$$n_x = \sin v,$$

$$n_y = \cos v \cos(q_0 x + u),$$

$$n_z = \cos v \sin(q_0 x + u). \tag{2}$$

Assuming only the fluctuating components of $n$ are contributing to the dielectric tensor for an optically uniaxial medium with anisotropy $\varepsilon_a = \varepsilon_\parallel - \varepsilon_\perp$, the fluctuating components of the dielectric tensor are

$$\varepsilon = \varepsilon_\perp I + \varepsilon_a nn,$$

$$\delta\varepsilon_{y,z} = \delta\varepsilon_{z,y} = \varepsilon_a(n_y{}^0 \delta n_z + n_z{}^0 \delta n_y) = \varepsilon_a u \cos(2q_0 x),$$

$$\delta\varepsilon_{x,y} = \delta\varepsilon_{y,x} = \varepsilon_a n_y{}^0 \delta n_x = \varepsilon_a v \cos(q_0 x),$$

$$\delta\varepsilon_{x,z} = \delta\varepsilon_{z,x} = \varepsilon_a n_z{}^0 \delta n_x = \varepsilon_a v \sin(q_0 x). \tag{3}$$

The Fourier transforms of these fluctuating components with respect to a scattering vector $k$ are

$$\delta\varepsilon_{y,z}(k) = \frac{\varepsilon_a}{2}[u(k+2q_0) + u(k-2q_0)],$$

$$\delta\varepsilon_{x,y}(k) = \frac{\varepsilon_a}{2}[v(k+q_0) + v(k-q_0)],$$

$$\delta\varepsilon_{x,z}(k) = \frac{\varepsilon_a}{2i}[v(k+q_0) - v(k-q_0)]. \tag{4}$$

Since the dielectric tensor is spatially modulated due to the helicoidal director structure, the scattering vector $k$ probes the fluctuations with wave vector $q = k \pm nq_0$, where $n=1$ for the "umbrella" mode ($v$), and $n=2$ for the "twisting" mode ($u$), and $q_0 = q_0\hat{x}$. We probe scattering vectors $k$ along ($k = k_x\hat{x}$) and perpendicular to the helical axis $k = k_\perp = q_\perp$.

### A. Cholesteric director along the helical axis (for a scattering vector $k = k_x\hat{x}$)

We have a thermal fluctuation wave vector $q = k_x\hat{x} \pm nq_0\hat{x} \equiv q_x\hat{x}$ and $q_y = q_z = 0$. The elastic free energy density is then expressed as

$$\begin{aligned}\delta F(r) = {} & \frac{K_1}{2}\left(\frac{\partial u}{\partial z}\cos q_0 x - \frac{\partial u}{\partial y}\sin q_0 x + \frac{\partial v}{\partial x}\right)^2 \\ & + \frac{K_2}{2}\left(\frac{\partial u}{\partial x} + \frac{\partial v}{\partial y}\sin q_0 x - \frac{\partial v}{\partial z}\cos q_0 x\right)^2 \\ & + \frac{K_3}{2}\left[\left(\frac{\partial u}{\partial y}\cos q_0 x + \frac{\partial u}{\partial z}\sin q_0 x + q_0 v\right)^2\right. \\ & \left. + \left(\frac{\partial v}{\partial y}\cos q_0 x + \frac{\partial v}{\partial z}\sin q_0 x\right)^2\right]\end{aligned} \tag{5}$$

to quadratic order in the fluctuations $u = u(r)$ and $v = v(r)$. Taking the Fourier transform to $q$ space and setting $q_y = q_z = 0$, we find a much simpler expression,

$$\delta F(q_x) = \frac{1}{2}K_2 q_x^2 u^2 + \frac{1}{2}(K_1 q_x^2 + K_3 q_0^2)v^2, \tag{6}$$

where $u = u(q_x)$ and $v = v(q_x)$, already in diagonal form, so that $u$ and $v$ individually correspond to the normal fluctuation modes of the cholesteric director. Applying the equipartition theorem gives

$$\langle |u(q_x)|^2 \rangle = \frac{k_B T}{K_2 q_x^2},$$

$$\langle |v(q_x)|^2 \rangle = \frac{k_B T}{K_3 q_0^2 + K_1 q_x^2}, \tag{7}$$

for the mean-square fluctuation amplitudes. The relaxation rates $\Gamma$ of the normal modes can be determined from the phenomenological dynamical equations

$$-\eta_1 \frac{\partial u}{\partial t} = \frac{\partial \delta F(q_x)}{\partial u},$$

$$-\eta_2\frac{\partial v}{\partial t}=\frac{\partial \delta F(q_x)}{\partial v}, \tag{8}$$

where $\eta_1$ and $\eta_2$ are damping parameters that incorporate the various viscosity coefficients in the system. Using Eq. (6) to evaluate the right-hand side of Eq. (8) and then taking a time dependence of the form $u,v$ and $e^{-\Gamma_u t}, e^{-\Gamma_v t}$, respectively, we obtain

$$\Gamma_u(q_x)=\frac{K_2 q_x^2}{\eta_1},$$

$$\Gamma_v(q_x)=\frac{K_3 q_0^2+K_1 q_x^2}{\eta_2}. \tag{9}$$

The fluctuation amplitudes may then be written as

$$\langle |u|^2\rangle = k_B T(\eta_1\Gamma_u)^{-1},$$

$$\langle |v|^2\rangle = k_B T(\eta_2\Gamma_v)^{-1}, \tag{10}$$

so that the amplitude is largest when the relaxation rate is smallest and slow fluctuations give rise to strong scattering. We may express the relaxation rates in terms of the scattering vector as the normal modes of an acousticlike or gapless $[\Gamma_u(q_x\to 0)\to 0]$ "twisting" mode $(u)$ and an opticlike or gapped $[\Gamma_v(q_x\to 0)\to \text{finite}]$ "umbrella" mode $(v)$:

$$\Gamma_u(k_x)=\frac{K_2(k_x\pm 2q_0)^2}{\eta_1},$$

$$\Gamma_v(k_x)=\frac{K_3 q_0^2+K_1(k_x\pm q_0)^2}{\eta_2}. \tag{11}$$

### B. Cholesteric director perpendicular to the helical axis (for a scattering vector $k=k_\perp=q_\perp$)

Here the calculation of the normal modes is considerably more complicated. A detailed analysis was carried out by Lubensky [12] for the case where $q_\perp$ is small compared to $q_0$ (e.g., a short pitch helix). Carrying out a perturbative calculation in the parameter $q_\perp/q_0$, Lubensky found the normal modes

$$\beta_+ = u+\frac{q_\perp}{q_0}v+O\left(\frac{q_\perp}{q_0}\right)^2,$$

$$\beta_- = v-\frac{q_\perp}{q_0}u+O\left(\frac{q_\perp}{q_0}\right)^2, \tag{12}$$

with relaxation rates given in terms of the scattering vector $k_\perp$ by

$$\Gamma_+(k_\perp)=\frac{4K_2q_0^2}{\eta_1}+\frac{K_+^{(1)}q_0^2}{\eta_1}\left(\frac{k_\perp}{q_0}\right)^2+\frac{K_+^{(2)}q_0^2}{\eta_1}\left(\frac{k_\perp}{q_0}\right)^4+O\left(\frac{k_\perp}{q_0}\right)^6,$$

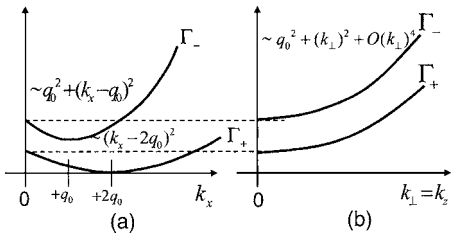


FIG. 2. The predicted dispersion relations of fast relaxation $\Gamma_-$ and slow relaxation $\Gamma_+$ at $k_x=q_0$ in an "ideal" cholesteric helix as a function of scattering vector: (a) in scattering geometry 1 ($k=k_x\hat{x}$) and (b) in scattering geometry 2 ($k=k_\perp=k_z=q_\perp$).

$$\Gamma_-(k_\perp)=\frac{(K_1+K_3)q_0^2}{\eta_2}+\frac{K_-^{(1)}q_0^2}{\eta_2}\left(\frac{k_\perp}{q_0}\right)^2+\frac{K_-^{(2)}q_0^2}{\eta_2}\left(\frac{k_\perp}{q_0}\right)^4+O\left(\frac{k_\perp}{q_0}\right)^6, \tag{13}$$

where $K_+$ and $K_-$ are combinations of ordinary nematic elastic constants $K_1$, $K_2$, and $K_3$. Note that these relaxation rates match up with $\Gamma_u$ and $\Gamma_v$ in Eq. (11) when $k=0$ (or $k_x=k_\perp=0$). Let us notice when $q_\perp=k_\perp\neq 0$, the normal modes are linear combinations of the "umbrella" and "twisting" modes. However, for $q_\perp\to 0$, the normal modes reduce to pure $u$ and $v$ as found for the case of fluctuations along the helical axis (i.e., for $q_x\neq 0, q_\perp=0$). Thus, we can use the normal modes of $\beta_+$ and $\beta_-$ for general thermal fluctuations $q$ and express the dielectric fluctuations in Eq. (3) in terms of these modes as

$$\delta\varepsilon_{y,z}(k)=\frac{\varepsilon_a}{2}\left[\beta_+(k\pm 2q_0)-\frac{k_\perp}{q_0}\beta_-(k\pm 2q_0)\right],$$

$$\delta\varepsilon_{x,y}(k)=\frac{\varepsilon_a}{2}\left[\beta_-(k\pm q_0)+\frac{k_\perp}{q_0}\beta_+(k\pm q_0)\right],$$

$$\delta\varepsilon_{x,z}(k)=\frac{\varepsilon_a}{2i}\left[\beta_-(k\pm q_0)+\frac{k_\perp}{q_0}\beta_+(k\pm q_0)\right]. \tag{14}$$

The scattering vector dependence of the relaxation rates $\Gamma_+$ and $\Gamma_-$ contains quartic (and higher) corrections when $k_\perp\neq 0$. As pointed out by Lubensky [12], this result occurs because of a remarkable cancellation of terms in the elastic free energy involving fluctuations in one of the components $(u,v)$ of the $\beta_+$ mode in one "Brillouin" zone [e.g., $(-q_0,q_0)$] and fluctuations of the other component in a neighboring zone. The schematic drawings of relaxation rates $\Gamma_\pm$ are plotted in Fig. 2 as functions of $k_x$ and $k_\perp$: For $k_x$ [in Fig. 2(a)], the plots are parabolas with the minima shifted away from $k_x=0$ due to an effect of the modulated or helicoidal structure along $x$. However, for $k_\perp$ [in Fig. 2(b)], the minima are at $k_\perp=0$, and there are possibly observable quartic corrections for large $k_\perp$. It suggests that the scattering vector defined by the experimental geometry and thermal fluctuation wave vector that is intrinsic to the system are the same for fluctuations off the helical axis ($q_\perp=k_\perp$), but differ modulo $q_0$ for fluctuations along the axis ($q_x=k_x\pm nq_0$).

## IV. DIRECTOR FLUCTUATIONS IN DISTORTED CHOLESTERICS

The director configuration is not a uniform sinusoidal helix due to a distorted helical state in the polymer-stabilized cholesteric diffraction gratings. The applied electric field reorients an initially undistorted helix, and the helical structure is somewhat distorted. The conceptual order and frustration in chiral liquid crystals are conclusively discussed by Kamien and Selinger [13]. In experiment, the relaxation modes of pure cholesteric and polymer-stabilized cholesteric liquid crystals are measured including the twist deformation [14]. We tested the helical distortion with a homeotropic cholesteric that has the helical twist extending in two directions: both along and perpendicular to the substrates. Since the helical twist along either direction is no longer describable by a pure sinusoidal, the generalization of the director can be then written as the sum of various fluctuating components. The corresponding generalization for the equilibrated and fluctuating components of director can be described as

$$
\begin{aligned}
n_x^0 &= 0, \\
n_y^0 &= \sum_n a_{yn} \cos(nq_0 x + \phi_{yn}), \\
n_z^0 &= \sum_n a_{zn} \sin(nq_0 x + \phi_{yn}), \\
\delta n_x &= v, \\
\delta n_y &= -u \sum_n a_{yn} \sin(nq_0 x + \phi_{yn}), \\
\delta n_z &= u \sum_n a_{zn} \cos(nq_0 x + \phi_{zn}).
\end{aligned} \tag{15}
$$

An ideal helix is unconstrained at the bounding surfaces, corresponding to $a_{y1}=a_{z1}=1$, $\phi_{y1}=\phi_{z1}=0$, and $a_{yn}=a_{zn}=0$ for $n\neq 1$. Then the relation between the fluctuation wave vector and the scattering vector in terms of $\beta_+$ and $\beta_-$ is

$$
\begin{aligned}
\delta\varepsilon_{y,z} &= \frac{\varepsilon_a}{2} \sum_{n,n'} a_{yn} a_{zn'} \left[ e^{\pm i\phi_{nn'}} \beta_+(k \pm (n+n')q_0) \right. \\
&\quad \left. - \frac{k_\perp}{q_0} e^{\pm i\phi_{nn'}} \beta_-(k \pm (n+n')q_0) \right], \\
\delta\varepsilon_{x,y} &= \frac{\varepsilon_a}{2} \sum_n a_{yn} \left[ e^{\pm i\phi_{yn}} \beta_-(k \pm nq_0) + \frac{k_\perp}{q_0} e^{\pm i\phi_{yn}} \beta_+(k \pm nq_0) \right], \\
\delta\varepsilon_{x,z} &= \frac{\varepsilon_a}{2i} \sum_n a_{zn} \left[ e^{\pm i\phi_{zn}} \beta_-(k \pm nq_0) + \frac{k_\perp}{q_0} e^{\pm i\phi_{zn}} \beta_+(k \pm nq_0) \right],
\end{aligned} \tag{16}
$$

where $\phi_{nn'} \equiv \phi_{y,n} - \phi_{z,n'}$.

In dynamic light scattering, the decay of the measured time correlation function of the scattered intensity, $\langle I(k,0)I(k,t)\rangle \langle \delta\varepsilon_{is}^*(k,0)\,\delta\varepsilon_{is}(k,t)\rangle^2$, will no longer correspond to a pair of pure exponential decays for normal modes of $\beta_+$ and $\beta_-$, but instead to a pair of broadened (or stretched) exponentials. This has the form [15]

$$
\langle I(k,0)I(k,t)\rangle = [A_+(k)e^{-[\Gamma_+(k)t]^{s_+}} + A_-(k)e^{-[\Gamma_-(k)t]^{s_-}}]^2 + B(k), \tag{17}
$$

where $s_\pm$ denotes exponents less than 1 that effectively spread the decays of the $\beta_+$ and $\beta_-$ modes over more than one fluctuation wave vector. The stretched exponential form has been extensively used in light scattering studies of polymer dynamics (where the broadening comes from a distribution of chain lengths or molecular weights) [16,17]. Therefore, the decay of the measured correlation function $\langle I(k,0)I(k,t)\rangle$ for a specific $k$ will then contain contributions from the fluctuations at $q=k\pm nq_0$ for the additional values of $n$. The mixing-in of these additional fluctuations could also contribute to the stretching of the exponential decays when the scattering vector has a component along the helical axis ($k=k_x$). In Fig. 3(a), the coupling of neighbor modes to additional $n$ will modify the measured behavior of the relaxation rates $\Gamma_\pm$ from that predicted for the distorted cholesteric state. The behavior of the relaxation rates $\Gamma_+$ and $\Gamma_-$ for scattering along the helical modulation axis ($x$) is quite different from that expected for an undistorted cholesteric. In particular, the overall minima in $\Gamma_+$ and $\Gamma_-$ occur for $k_x \to 0$; $\Gamma_+$ appears to be nearly gapless ($\Gamma_+ \to 0$) at $k_x=0$. However, *local* minima are observed in $\Gamma_+$ and $\Gamma_-$ at the same scattering vector $k_x=2q_0=3.8\ \mu\text{m}^{-1}$ and possibly weakly in $\Gamma_-$ at $k_x=q_0\approx 1.9\ \mu\text{m}^{-1}$. The observed features in the dispersion are in fact more consistent with the model in Fig. 3(b), in which the effect of a distortion with a significant uniform component to the director configuration was considered. Indeed, the lowest-energy twist distortions of the ideal helix come from the $n=0$ (uniform) and $n=2$ terms in Eq. (15). (The $n=1$ term describes an undistorted helix, which has zero elastic energy.) The distortion terms contribute a twist elastic energy density that scales as

$$
K_2 \left( n_z^0 \frac{\partial n_y^0}{\partial x} - n_y^0 \frac{\partial n_z^0}{\partial x} + q_0 \right)^2 K_2 (n-1)^2 q_0^2,
$$

which is lowest (except for $n=1$) when $n=0,2$. A significant presence of these terms then implies from Eq. (10) that strong scattering can be expected from the modes $\beta_\pm(k_x)$, with minimum relaxation rate $\Gamma_\pm$ (and correspondingly large amplitude) at $k_x=0$—whose effect is shown in Fig. 3(a) and from $\beta_-(k_x-2q_0)$ with minimum $\Gamma_-$ (and large amplitude) centered at $2q_0$, in addition to the modes $\beta_+(k_x-2q_0)$ and $\beta_-(k_x-q_0)$ expected for an undistorted helix. The solid lines in Fig. 3(b) represent the fits of the relaxation rates $\Gamma_\pm$ to the predictions, for $q_x=k_x\pm nq_0$ ($n=0$, 1, or 2) and for ranges of the scattering vector $k_x$ restricted around the appropriate local minima (0, $q_0$, or $2q_0$). Clearly, the latter fits are inadequate, and the best model for the data corresponds to a significantly distorted helical structure, with the $n=0$ and $n=2$ terms in the harmonic expansion for $n$ [Eq. (15)] being prominent.

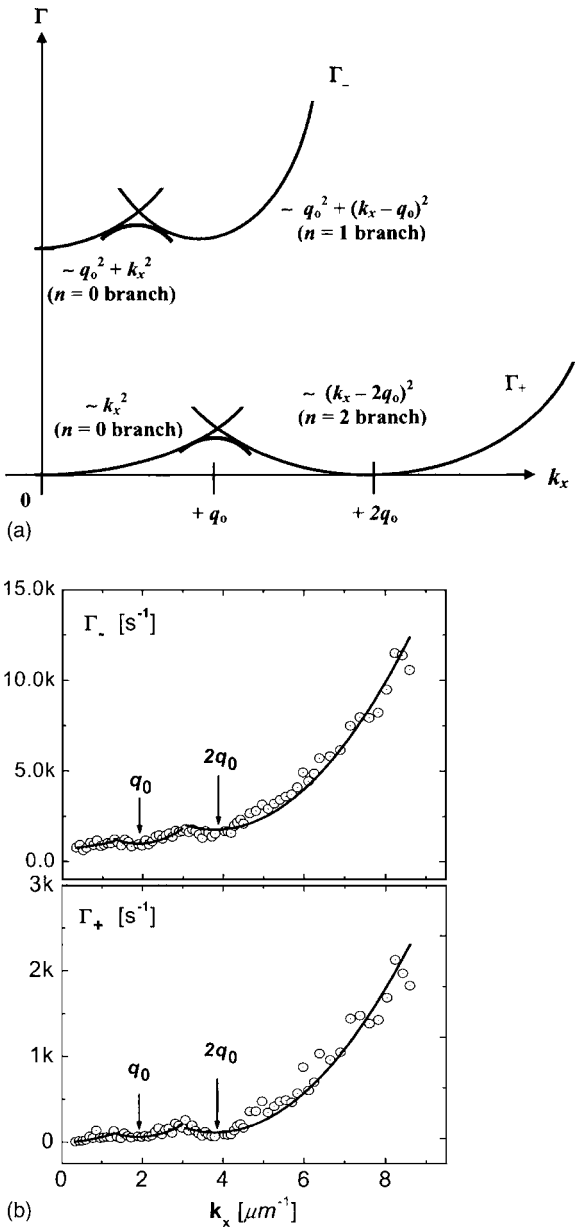


FIG. 3. (a): Predicted dispersion as a function of scattering vector along the helical axis ($k=k_x$) of a distorted cholesterics containing significant amplitudes for $n=0$ and $n=1$, and $n=2$ terms in Eq. (19). By contrast, for an undistorted cholesterics we expect overall minima at $k_x=2q_0$ for slow relaxation $\Gamma_+$ and at $k_x=q_0$ for fast relaxation $\Gamma_-$ [see in Fig. 2(a))]. (b): Experimental dispersion of both for slow relaxation $\Gamma_+$ and fast relaxation $\Gamma_-$ rates as a function of scattering vector along the helical axis ($k=k_x$) of a distorted cholesterics. The special scattering vectors $k_x=q_0=1.9\ \mu\mathrm{m}^{-1}$ and $k_x=2q_0=3.8\ \mu-^1$, which correspond to $2\pi$ and $4\pi$ variations in the phase of the director, are also indicated.

From the typical data for the correlation function $\langle I(k,0)I(k,t)\rangle$, together with fits to various exponential decays for the specific geometry, $\theta_i'=0$, $\theta_s'=58$, and $k\approx k_x=8.4\ \mu\mathrm{m}^{-1}$, we have found a good fit to the data by allowing for a spread in the relaxation rates of the modes via a stretched exponential decay due to the effect of distortion. This can be achieved by stretching only the slower mode ($\beta_+$)—i.e., fixing $s_-\equiv 1$ and varying $s_+$. The residuals for this fit are now comparable to the statistical noise in the shortest time channels, and no further improvement could be achieved by independently stretching both modes. From our fitting we find $s_+=0.70-0.75$ for all values of $k_x$ over the range $0.5-9\ \mu\mathrm{m}^{-1}$ probed. From a similar fitting of the correlation data for different combinations of $\theta_i'$, $\theta_s'$, the result is shown in Fig. 3(b). The special scattering vectors $k_x=q_0=1.9\ \mu\mathrm{m}^{-1}$ and $k_x=2q_0=3.8\ \mu\mathrm{m}^{-1}$, which correspond to $2\pi$ and $4\pi$ variations in the phase of the director, are also indicated.

## V. DISTORTED CHOLESTERICS IN A MESOGENIC VS ISOTROPIC POLYMER NETWORK

The distorted cholesterics in a polymer-containing matrix is unlike the case of a pure cholesteric confined between homeotropic substrates. The main agent causing distortion of a simple cholesteric structure in polymer-stabilized samples is an applied electric field that reorients the helical structure from a "normal" state (helical axis normal to substrates treated for homogeneous alignment that minimize distortion when the cell thickness $\gg$ helical pitch) to a "fingerprint" state (significant component of the helical axis in the substrate plane). The internal polymer network in polymer-stabilized samples locks in this fingerprint state. The difference between the polymer network morphologies for mesogenic RM257 and isotropic HDDA networks is shown with the anchoring of polymer walls to the cholesteric director [10,11]. The RM257 network shows a high degree of spatial patterning and a highly orientationally ordered fibril structure extending across the sample thickness. By contrast, the HDDA network shows relatively weak spatial patterning and no clear orientational order of the fibrils—in fact, it appears that the network structure has collapsed onto the substrate when the cell was opened for Scanning tunneling microscopy (SEM). In addition to the impact on the scattering due to distortion of the pure helical state, the polymer network will introduce qualitatively new effects: One of these is the possibility of a slow relaxational mode arising from local motion of polymer fibrils not completely frozen into the large, rigid bundles, consequently coupled to the surrounding liquid crystal, inducing slow director fluctuations and thus fluctuations of scattered light intensity because of the dielectric contrast between the polymer and liquid crystal. We would expect this "polymer mode" to contribute a significantly stretched exponential decay due to the polydispersity in fibril size in the measured time correlation function of the scattered intensity. Another potential consequence of the polymer network is more interesting—namely, the possibility of a patterned distribution of dense, narrowly spaced polymer walls producing a confinement effect on the director fluctuations between the walls. The controllable, orientational templating effect of the liquid crystal host on the developing network during polymerization presents a unique method for tailoring anchoring conditions in a confined liquid-crystal system. A phenomenological model is presented by Crawford and co-workers in polymer-stabilized nematic liquid crystals, where polymer fibrils from the direc-

tor domains are constrained with a finite anchoring energy [18,19].

In this report, we propose a possible model of confinement effects to distorted cholesterics: Suppose the scattering from a stack of nematic slabs confined between two rigid substrates with separation $L_x$ and treated for strong homogeneous anchoring at the surfaces. We shall also assume the sample is effectively unbounded in the $y$ and $z$ directions. The scattered intensity for scattering vector $k$ is given by

$$\langle I(k,t)\rangle = \left(\frac{E_0\omega^2}{4\pi c^2 R}\right)^2 \left\langle \left| \int_{V_{scatt}} e^{-ik\cdot r}\varepsilon_{if}(r,t)dr \right|^2 \right\rangle, \quad (18)$$

where

$$\varepsilon_{if}(r,t) = \varepsilon_{0,if} + \delta\varepsilon(r,t) = \varepsilon_{0,if} + \sum_q e^{iq\cdot r}\delta\varepsilon_{if}(q,t) \quad (19)$$

and $E_0$ and $\omega$ are the amplitude and frequency of the incident electric field, $R$ is the distance from the scattering (or illuminated) volume $V_{scatt}$ to the detector, and $\varepsilon_{if}$ is the detected component of the dielectric tensor. The angular brackets represent a time average over the photocurrent generated in the detector. Then the integrals over $y$ and $z$ (the unbounded directions) give

$$\langle I(k\neq 0,t)\rangle = \left(\frac{E_0\omega^2}{4\pi c^2 R}\right)^2 N \left\langle \left| \sum_{q_x} \delta\varepsilon_{if}(q_x,k_y,k_z,t)\frac{\sin(q_x-k_x)L_x/2}{(q_x-k_x)L_x/2} \right|^2 \right\rangle, \quad (20)$$

where $N$ represents the number of nematic slabs in the stack that are illuminated. The fluctuations in two different slabs are assumed to be uncorrelated (i.e., the substrates or walls isolate the slabs). In our actual experiments, the slabs have submicron thickness, so that typically $\sim$100 slabs are illuminated. The uniform part of the dielectric tensor $\varepsilon_{0,if}$ only contributes to scattering in the forward direction ($k=0$) and therefore does not appear in Eq. (20). Due to the fixed boundary conditions at the slab surfaces, the fluctuation wave vector component $q_x$ takes on discrete values $n\pi/L_x$, where $n=\pm 1,\pm 2,\ldots$. Putting this into Eq. (19) we finally obtain

$$\langle I(k\neq 0,t)\rangle = \left(\frac{E_0\omega^2}{4\pi c^2 R}\right)^2 N \sum_{m,n\neq 0} \langle \delta\varepsilon^*_{if}(m\pi/L_x,k_y,k_z,t) \times \delta\varepsilon_{if}(n\pi/L_x,k_y,k_z,t)\rangle \times \frac{\sin(m\pi-k_xL_x)/2}{(m\pi-k_xL_x)/2}\frac{\sin(n\pi-k_xL_x)/2}{(n\pi-k_xL_x)/2}. \quad (21)$$

This result exposes a potentially interesting consequence of confinement on the scattering. We see that when the slab thickness is comparable to the optical length scales probed in the experiment [so that the integral $\int_{-L_x/2}^{L_x/2} e^{i(q_x-k_x)x}dx$ that is encountered after substituting Eq. (19) into Eq. (18) is *not* effectively a $\delta$ function], the scattering vector need not match any fluctuation-mode wave vector, and several modes can contribute to the scattering for fixed $k_x$. However, the oscillating function on the bottom line of Eq. (21) is sharply peaked around $k_x=n\pi/L_x=m\pi/L_x$, so when $k_x<\pi/L_x$ (or $k_x>-\pi/L_x$), only the term $n=m=1$ (or $n=m=-1$) contributes significantly in the sum. Consequently, for $-\pi/L_x<k_x<\pi/L_x$ and $k_y=k_z=0$, the scattering essentially comes only from the fluctuations with $|k_x|=\pi/L_x$. This means that the dispersion of the relaxation rates associated with the confined fluctuations will flatten or be "cut off" inside scattering vector $|k_x|\pi/L_x$—i.e., $\Gamma(k_x)$ will become approximately constant in $k_x$. In the case of an acousticlike fluctuation that is gapless at $k_x=0$ in a bulk sample [e.g., $\Gamma(k_x)Kk_x^2/\eta$], a gap will appear in the confined sample [e.g., $\Gamma(k_x\to 0)\to K(\pi/L_x)^2/\eta$]. Physically, one can say that longer-wavelength fluctuations get "cut off" by the combination of a narrow spacing between confining walls and the surface anchoring conditions. On the other hand, when $|k_x|>\pi/L_x$, higher-fluctuation wave vectors ($n$, $m>1$ or $n$, $m<-1$) are significantly sampled and $\Gamma(k_x)$ begins to increase. The initial increase can be shown to be roughly quadratic. Figure 4 shows a comparison of typical correlation functions for the scattering geometry corresponding to geometry 1 (with $k=k_x=9.25\ \mu\text{m}^{-1}$) and geometry 2 (with $k=k_z\sim 9.10\ \mu$m) of cholesterics-stabilized with mesogenic (RM257) and isotropic (HDDA) polymer networks. The striking feature of the comparison is the broad slow tail present at longer delay

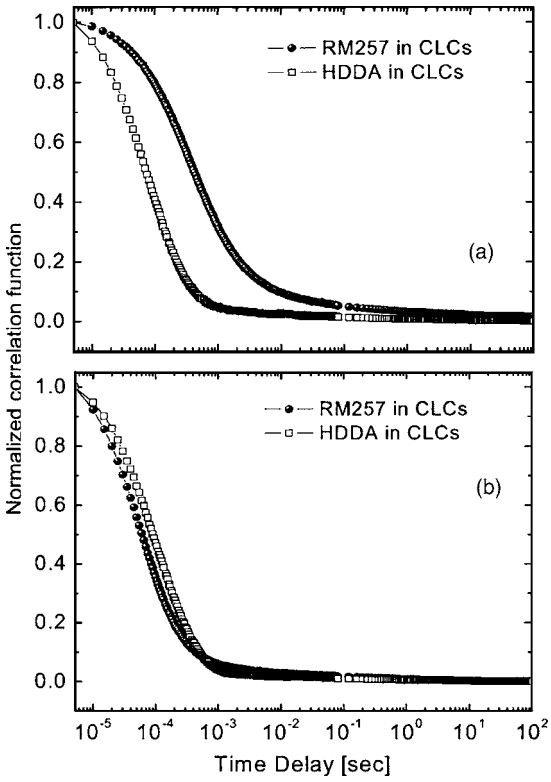


FIG. 4. Typical normalized intensity autocorrelation functions: (a) for scattering geometry 1 at $k_x\sim 9.25\ \mu\text{m}^{-1}$ and (b) for scattering geometry 2 at $k_z\sim 9.10\ \mu\text{m}^{-1}$. Results are shown for two different types of polymer networks (using reactive mesogenic RM257 and isotropic HDDA) in a cholesteric liquid-crystal director. The contribution from the amplitude of slow mode in a reactive mesogenic polymer network (RM257 in cholesterics) is dramatically shown in the scattering geometry 1.

times on the mesogenic RM257 network, relative to the flat background observed for the pure cholesterics at similar decay times. The broad, slow component of correlation functions is the evidence of the "polymer" mode (and its coupling to director fluctuations) predicted at the beginning of the previous section. When we compared experimental results with several trial fitting functions, we found significant improvements of fits using two (fast-slow cholesterics director) modes and one stretched "polymer" mode. The reason for this is that the distortion of an ideal helix within either a mesogenic or isotropic polymer network can be coupled with the slow mode of the cholesteric director fluctuations along the helical axis. Interestingly the amplitude of the "polymer" mode appears to be much pronounced when the scattering is observed along the twist axes—i.e., for scattering geometry 1. However, for scattering geometry 2 (where scattering is off the twist axis), there is only one stretched "polymer" mode. Thus the averaged scattered intensity fluctuation $\langle I(k,0)I(k,t)\rangle$ is supplemented by an additional term $A_p(k)e^{-[\bar{\Gamma}_p(k)t]^{s_p}}$, where the stretching exponent $s_p$ characterizes the observed broad decay of the polymer mode ($s_p \sim 0.2 \ll 1$). Although isotropic HDDA data can be described with no stretch mode of both fast-slow cholesterics director modes ($s_+ = s_- = 1$), the mesogenic RM257 data were best fit with the slow mode ($s_+ \sim 0.7$), with a relatively "suppressed" relaxation rate (6.0 $\text{sec}^{-1}$) compared to an isotropic HDDA network (6.0 $\text{sec}^{-1}$).

## VI. EXPERIMENTAL RESULTS

### A. Dispersion of relaxation rates of distorted cholesterics in a mesogenic polymer network

The scattering vector dependence of the director mode of relaxation rates $\Gamma_+$ and $\Gamma_-$ of distorted cholesterics in a mesogenic (RM257) polymer network is plotted in Fig. 5. The rates were extracted from the fits to the correlator data described in the previous section. Let us first consider the dispersion for $k=k_x$ (along the grating axis in the optical texture). For a scattering vector for $k_x \geq 7\ \mu\text{m}^{-1}$, which is approximately 3 times the wave vector $\pi/L_x \sim 2.5\ \mu\text{m}^{-1}$ corresponding to the spacing $L_x$ between polymer walls, $\Gamma_+$ and $\Gamma_-$ increase in a roughly quadratic fashion. On the other hand, as the bottom panel of the figure particularly shows, for $k_x \leq 7\ \mu\text{m}^{-1}$ the relaxation rates are approximately flat (independent of $k_x$), all the way down to the lowest $k_x$ where we could reliably measure the correlation function. Furthermore, extrapolating $\Gamma_+$ to $k_x=0$ indicates a gap of about 150 $\text{sec}^{-1}$ in the $\beta_+$ director mode. Although the effect of helical distortion for the homeotropic sample is to substantially alter the $k_x$ dependence of the relaxation rates due to coupling to branches of the dielectric fluctuations centered on multiples of the helical wave vector other than $n=1$, the dispersion in the homeotropic case is certainly not flat and the acoustic mode does appear to extrapolate to zero relaxation rate at $k_x=0$. Instead of being a pure effect of the coupling to other fluctuation branches, the $k_x$ dispersion for the mesogenic RM257 network has the additional features of confined fluctuations discussed in the previous section—

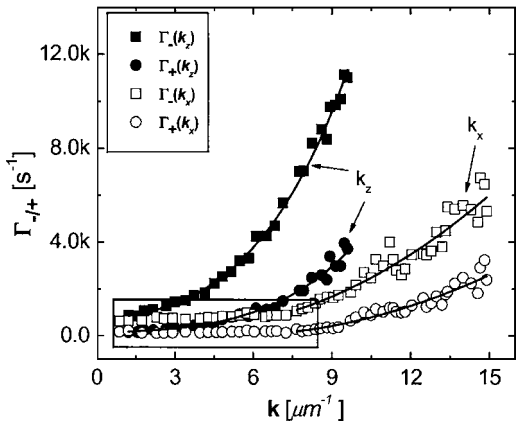


FIG. 5. Scattering vector dependence of relaxation rates for the *distorted* cholesteric helix in a mesogenic RM257 network: The fast mode ($\Gamma_-$) and slow mode ($\Gamma_+$) increase in a quadratic fashion for scattering geometry 2. For scattering geometry 1, however, such a quadratic dependence is only found for wave vectors $k_x \geq 7\ \mu\text{m}^{-1}$, which is approximately 3 times the wave vector $\pi/L_x \sim 2.5\ \mu\text{m}^{-1}$ corresponding to the spacing $L_x$ between polymer walls. For $k_x \leq 7\ \mu\text{m}^{-1}$ the relaxation rates in geometry 1 are approximately flat or independent of $k_x$ (see the rectangular region inside figure) all the way down to the lowest $k_x$ where we could reliably measure the correlation function.

specifically, a "cutoff" for smaller values of $k_x$. In the case of a confined cholesteric, the cutoff condition $-\pi/L_x < k_x < \pi/L_x$ discussed in the previous section for a uniform nematic becomes $-\pi/L_x < k_x - nq_0 < \pi/L_x$ for each separate branch $n$ of the dielectric fluctuations that contributes significantly to the scattering. If we assume that the significant branches are those that cost the least twist energy, $n=0$, 1, 2 (as was the case for the homeotropic cholesterics, the positive $k_x$ cutoff would be $k_x \sim 2q_0 + \pi/L_x$. Using $q_0 = \pi/\text{optical pitch} \approx 2.5\ \mu\text{m}^{-1}$ and $L_x = 1.2\ \mu\text{m}$, we get $k_x = 7.5\ \mu\text{m}^{-1}$, which agrees well with the observed cutoff point in Fig. 5.

Another interesting indication of a confinement effect in the mesogenic RM257 network relative to the pure cholesterics is the visualization of the slow fluctuations in the scattered intensity around $k_x \approx 2q_0$. This means the predicted $(k_x - 2q_0)^2$ dependence of the relaxation rate for the $\beta_+$ mode that arises because of the twisted cholesteric structure. Specifically, very slow fluctuations should be observed for $k_x \approx 2q_0$, where the corresponding fluctuation wave vector $q_x = k_x - 2q_0$ vanishes. However, none of the diffraction orders observable in the RM257 network (including the zero-order, undiffracted beam at $k_x=0$) showed visibly slow fluctuations surrounding the central spot—evidently small values of $q_x$ are "cut off" in this case, which agrees with the expected effect of the confinement and strong anchoring by the polymer walls. For geometry 2, the dominant component is in the direction parallel to both the polymer walls and the substrates—i.e., the "unbounded" direction of our sample. We then expect no confinement effect, and further, since the scattering vector is now normal to the director modulation, no effect due to coupling among different branches of the dielectric fluctuations is observed. Indeed, this is what is

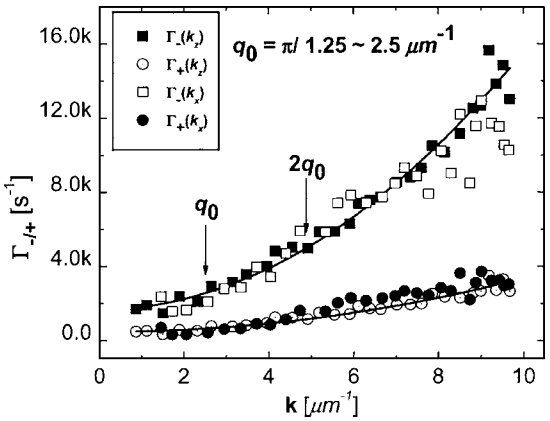


FIG. 6. Scattering vector dependence of relaxation rates, fast mode ($\Gamma_-$) and slow mode ($\Gamma_+$), for the *distorted* cholesteric helix in an isotropic HDDA network: Although the spacing $L_x$ between polymer walls is the same as $\pi/L_x \sim 2.5\ \mu\mathrm{m}^{-1}$ corresponding to mesogenic RM257 network, the slow-mode relaxation rate $\Gamma_+$ is approximately degenerate or "overlapped" between the two scattering geometries, $k=k_x$ and $k=k_z$, and is described by a simple quadratic dependence on scattering vector $k$.

observed. Both $\Gamma_+$ and $\Gamma_-$ rise monotonically from $k_z=0$, and there is no flattening or secondary minima in their dependence on $k_z$. We also may expect a significant quartic contribution to the dependence of $\Gamma_+$ on $k_z$ in addition to the quadratic term. In fact, as the fits demonstrate, a quadratic plus quartic dispersion does seem to account for the curvature of $\Gamma_+$ and $\Gamma_-$ better than a pure quadratic term.

### B. Dispersion of relaxation rates of distorted cholesterics in an isotropic polymer network

Figure 6 is a plot of the dispersion of the modes obtained for the isotropic HDDA network, and the results are quite different from the case of the mesogenic RM257 network. Both relaxation rates $\Gamma_+$ and $\Gamma_-$ are approximately degenerate between the two scattering geometries $k=k_x$ and $k=k_z$, and described by a simple quadratic dependence on scattering vector $k$. It turned out that the isotropic HDDA morphology does not appear nearly as efficient as the mesogenic RM257 morphology in terms of capturing and anchoring the electric-field-distorted state of the cholesterics. We propose that in the HDDA case, the distorted state relaxes when the electric field is removed and further into a state in which there is a significant polydispersity in the orientation of the local helical axis. This would be somewhat analogous to the so-called "scattering state" of a polymer-stabilized cholesterics display (except that the $d/p_0$ ratio in the latter is typically much greater than 1). Assuming a polydisperse distribution of the twist direction, one would anticipate a much higher degree of degeneracy in the director scattering along the two directions $k_x$ and $k_z$. For whichever is the case, we would not expect significant spatial confinement effects on the fluctuations in the isotropic HDDA network, which is more porous and weakly orientationally ordered. Furthermore, if the local helical structure has relaxed back to the lowest-elastic-energy state [$n=1$ term in Eq. (14)], there would be no distortion effects of the type (unlikely described in the mesogenic RM257 network), and this would explain the absence of cholesterics distortion effects on the dispersion and the lack of a need for a stretched exponential to describe the correlation function in the HDDA case in Fig. 6.

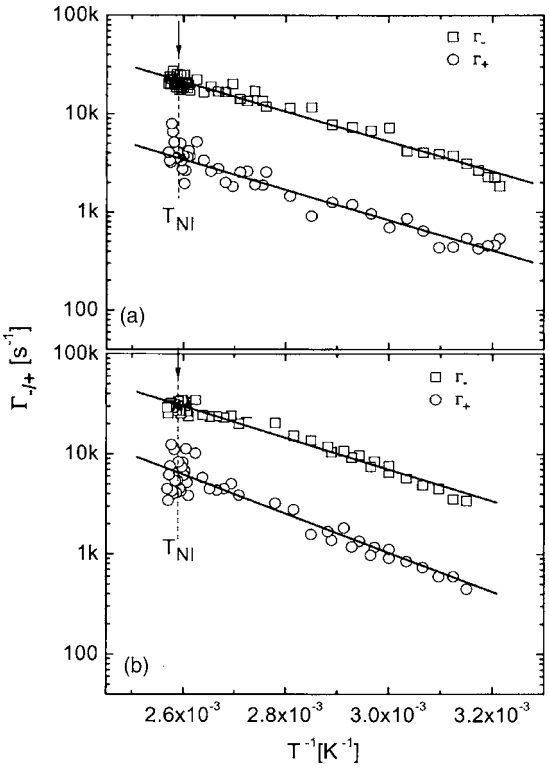


FIG. 7. Temperature dependence of fast-mode ($\Gamma_-$) and slow-mode ($\Gamma_+$) relaxation in cholesteric liquid crystals: (a) for a mesogenic RM network and (b) for an isotropic HDDA network.

### C. Temperature dependence of the relaxation rates of distorted cholesterics in a mesogenic vs isotropic polymer network

We also measured the temperature dependence of $\Gamma_+$ and $\Gamma_-$ for both mesogenic and isotropic polymer networks. The samples are tested for scattering geometry 1 corresponding to $k=k_x=4.5\ \mu\mathrm{m}^{-1}$, and their results are shown in Fig. 7, where $\Gamma$ is plotted on a semilogarithmic plot against the inverse of the absolute temperature. The range of temperature is 25–115 °C or about 2.5 °C above the nematic-to-isotropic transition in the pure cholesteric mixture. The plot reveals an Arrhenius-type behavior, which is quite common for viscosity coefficients $\eta=\eta_0 \exp(E_0/k_BT)$ associated with director fluctuations in liquid crystals. We have fit our data with $\Gamma_\pm=\Gamma_\pm^0 \exp(-E_\pm^0/k_BT)$, which gives $\Gamma_-^0=5432\ \mathrm{sec}^{-1}$, $E_-^0=2.21\times10^{-13}$ erg and $\Gamma_+^0=6836\ \mathrm{sec}^{-1}$, $E_+^0=2.67\times10^{-13}$ erg for the isotropic HDDA network. For a mesogenic RM257 network, we have found $\Gamma_-^0=4024\ \mathrm{sec}^{-1}$, $E_-^0=2.10\times10^{-13}$ erg and $\Gamma_+^0=1882\ \mathrm{sec}^{-1}$, $E_+^0=2.13\times10^{-13}$ erg. These activation energies are probably related to the rotational viscosity or molecular moment of inertia depending on the molecular shape, length scale, and temperature [20]. Reorientation of the cholesteric director in the polymer network is

somewhat slower—i.e., "suppressed"—as compared to than pure twist cholesterics and reorientation of nematic liquid crystals. Our results in Fig. 7 imply at most a weak temperature dependence of the elastic constants $K$ over the range studied. There is an absence of a clear anomaly in the temperature dependence of $\Gamma$ at the $N^*$-$I$ transition of the pure liquid crystal, which probably indicates an upward shift in the transition temperature of both the mesogenic and isotropic networks in the cholesterics phase. It would be useful to carry out measurements at higher temperature close to the transition temperature.

## VII. SUMMARY AND DISCUSSION

To close, we would like to comment on some possibilities for future research such as the attractiveness of the polymer-stabilized system for confinement studies, the combination of spatial patterning with an orientational templating effect, and the self-organization of not only a well-defined spatial array of confining surfaces or walls, but also imparting a variable degree of orientational order into these surfaces. We have shown the dynamics of distorted cholesterics in both mesogenic and isotropic polymer networks with two scattering geometries. The confinement can probe the crossover from the confined direction to the "unbounded direction" by choosing a "convenient" scattering geometry depending on the system. In principle, the control of defining the confinement matrix and spacing between walls, including the strength of anchoring at the walls, can be tuned. However, the main disadvantages of polymer-stabilized systems are the complex director configuration, which significantly complicates quantitative interpretation of the results, and the difficulty in achieving defect-free distorted cholesterics templates with submicron pitch. Ideally, one would like to vary the confinement length scale from $\sim 0.2\lambda$ to $\sim 4\lambda$, where $\lambda$ is a convenient wavelength in the visible range (e.g., 0.633 $\mu$m). The solution to these two problems could be the use of uniform, homeotropically aligned nematics (which has the simplest possible director configuration) in place of the cholesterics and impose spatial templating of the polymer network by external means—in particular, by two-beam interference—to produce a periodic, stationary intensity distribution that would then lead to a spatially templated photopolymerization process. If a UV laser is used, one could produce subvisible spacings between polymer walls. The challenge would be to tune the polymerization process (UV intensity, exposure protocol) and materials (monomer and initiator concentrations, relative monomer–liquid-crystal diffusion constants, etc.) in order to ultimately produce sharply defined walls.

## ACKNOWLEDGMENTS

This research was supported by the Office of Naval Research under Grant No. N00014-99-1-0899 and by ALCOM/NSF under Grant No. DMR-8920147. K.K. gratefully thanks Professor Gerhard Nagele and Professor Jan K.G. Dhont for reading this manuscript.

[1] P. V. Shibaev, V. I. Kopp, and A. Z. Genack, J. Phys. Chem. **107**, 6961 (2003).
[2] V. I. Kopp and A. Z. Genack, Phys. Rev. Lett. **86**, 1753 (2001).
[3] A. Y.-G. Fuh, T.-H. Lin, J.-H. Liu, and F.-C. Wu, Opt. Express **12**, 1857 (2004).
[4] R. M. J. Cotterill, *Biophysics: An Introduction*, (Wiley, New York, 2002).
[5] C. Xu, P. Taylor, M. Ersoz, P. D. I. Fletcher, and V. N. Paunov, J. Mater. Chem. **13**, 3044 (2003).
[6] P. G. de Gennes and J. Prost, *The Physics of Liquid Crystals*, 2nd ed. (Clarendon, Oxford, 1993).
[7] R. B. Meyer, Appl. Phys. Lett. **12**, 281 (1968).
[8] S. V. Shiyanovskii, I. I. Smalyukh, and O. D. Lavrentovich, *Defects in Liquid Crystals: Computer Simulations, Theory and Experiments*, (Kluwer Academic, Dordrecht, 2001).
[9] S. Lee, L. C. Chien, and S. Sprunt, Appl. Phys. Lett. **72**, 885 (1998).
[10] S. Kang, S. Sprunt, and L. C. Chien, Appl. Phys. Lett. **76**, 3516 (2000).
[11] K. Kang, L. C. Chien, and S. Sprunt, Liq. Cryst. **29**, 9 (2002).
[12] T. C. Lubensky, Phys. Rev. A **6**, 452 (1972).
[13] R. D. Kamien and J. V. Selinger, J. Phys.: Condens. Matter **13** R1 (2001).
[14] R. Borsali, U. P. Schroeder, D. Y. Yoon, and R. Pecora, Phys. Rev. E **58**, R2717 (1998).
[15] M. S. Spector, MIT thesis, "Light Scattering from Thin Smectic Liquid Crystal Flims," Feb. 1993.
[16] V. Degiorgio, R. Piazza, F. Mantegazza, and T. Bellini, J. Phys.: Condens. Matter **2**, SA69 (1990).
[17] R. A. L. Vallee, M. Cotlet, J. Hofkens, F. C. De Schryver, and K. Mullen, Macromolecules (to be published).
[18] G. P. Crawford, A. Scharkowski, Y. K. Fung, J. W. Doane, and S. Zumer, Phys. Rev. E **52**, R1273 (1995).
[19] P. A. Kossyrev, J. Qi, N. V. Priezjev, R. A. Pelcovits, and G. P. Crawford, Appl. Phys. Lett. **81**, 2986 (2002).
[20] S. Gauza, H. Wang, C.-H. Wen, S.-T. Wu, A. J. Seed, and R. Dabrowski, Jpn. J. Appl. Phys., Part 1 **42**, 3463 (2003).